J Mater Sci: Mater Med (2008) 19:1389–1397
DOI 10.1007/s10856-007-3261-9

# Synthesis and hydrothermal treatment of nanostructured hydroxyapatite of controllable sizes

**Say Chye Joachim Loo · Yiwei Eva Siew · Shuhui Ho · Freddy Yin Chiang Boey · J. Ma**

Received: 10 July 2006 / Accepted: 14 August 2007 / Published online: 4 October 2007


**Abstract** Nanoparticulate systems have been studied for targeted and controlled release of therapeutic agents; and size is one of the major determinants of their in vivo clearance kinetics by the MPS macrophages. As such, it is important to control the size of hydroxyapatite nanoparticles during synthesis. The results show that the size of hydroxyapatite nanoparticles, synthesized through chemical precipitation, increases with increasing synthesis time. Particle sizes were also observed to increase in a linear correlation with temperature. Crystallinity and carbonate-substitution of the nanoparticles also increased with temperature. Hydrothermal, performed as a post-synthesis treatment, improves particle morphology, giving particles with regular surface contours, well-defined sizes and lower particle agglomeration. By controlling synthesis temperature and time, hydroxyapatite nanoparticles with well-defined sizes and morphology can be obtained.

## 1 Introduction

Hydroxyapatite has been widely used for biomedical applications owing to its similarity in mineral constituents with human hard tissues (bones and teeth) [1]. The use of hydroxyapatite, in particulate systems or as nanoparticles, as a carrier for drug [2], protein [3], enzyme [4] and plasmid DNA [5] has also been well documented. Particulate systems for the delivery and application of drugs and other therapeutic agents are claimed to have enhanced bioavailability, predictable therapeutic response, greater efficacy and safety, and controlled and prolonged release time [6]. As such, the employment of hydroxyapatite nanoparticles for targeted and controlled release of therapeutic agents (targeted-delivery) in biomedical applications is showing to be promising.

The main problem of particulate systems remains to be the efficient uptake of these nanoparticles by the mononuclear phagocyte system (MPS) macrophages in vivo; and size is one of the major determinants of clearance kinetics of these nanoparticles by the MPS macrophages [7, 8]. Therefore, it is imperative that the particle size of hydroxyapatite nanoparticles be well controlled during synthesis, especially for particulate systems in targeted-delivery applications. Nano-sized particles of hydroxyapatite can be obtained by an appropriate synthesis technique [9–16], but the ability to accurately control and achieve various sizes of hydroxyapatite nanoparticles remains a challenge.

Although many routes have been explored for the synthesis of hydroxyapatite nanoparticles, the chemical precipitation route has proven to be popular, because of its versatile and economical advantages, and thus has been extensively reported [9–16]. The effects of synthesis temperature [10, 12–14[e1]], time [9, 10], calcium ion concentration [13], surfactant [15], calcination [9, 10] and the use of different reagents [16], on the morphological properties of hydroxyapatite nanoparticles through this synthesis route have been studied, but the results so far have been varied. Conflicting results have been obtained for the effect of synthesis temperature on particle size. Pang and Bao [10] and Kumar et al. [12] both reported the increase in particle size of hydroxyapatite with increasing synthesis temperature; but on the contrary, Cao et al. and

S. C. J. Loo (✉) · Y. E. Siew · S. Ho · F. Y. C. Boey · J. Ma
School of Materials Science and Engineering,
Nanyang Technological University, Nanyang Avenue,
Singapore 639798, Singapore
e-mail: joachimloo@ntu.edu.sg

Bouyer et al. [13, 14] reported a decrease in particle size with increasing synthesis temperature. Interestingly, Cao et al [13] also reported that the calculated crystallite size, using Scherrer's equation, of their synthesized hydroxyapatite nanoparticles was actually vastly different from the transmission electron microscope (TEM) sizes; in which the calculated crystallite size was much smaller than the observed TEM size, though no explanation was given. Nevertheless, it was commonly observed from these papers that the particles synthesized through chemical precipitation are often highly agglomerated, which according to Rahaman's classification [17], these agglomerates could be clusters of ultra-fine primary particles [9].

As such, a more rigorous measurement of particle size is required. Measurement of hydrodynamic sizes of well-dispersed particles using dynamic light scattering (DLS) would therefore be a good complimentary alternative for particle sizing. The requirement for accurate particle sizing using DLS is therefore, a well-dispersed and stable colloid of hydroxyapatite nanoparticles. Various dispersants have been studied for the dispersion of hydroxyapatite nanoparticles. Welzel et al. [11] has briefly reported the use of cationic, anionic and non-ionic organic dispersants, namely cetyltrimethylammonium bromide (CTAB), sodium dodecyl sulphate (SDS) and octylphenoxy polyethoxyethanol (Triton X-100), though preliminary studies have shown them to be less than effective. As such, we are proposing the use of a more effective inorganic dispersant in sodium hexametaphosphate (SHMP) to disperse these nanoparticles before their hydrodynamic sizes are measured.

The objective of this paper is to report on how synthesis temperature and time can affect the size of hydroxyapatite nanoparticles, and how these synthesis parameters can be manipulated to tailor various sizes of nanostructured hydroxyapatite particles. Here, hydroxyapatite nanoparticles would be synthesized through chemical precipitation, and hydrothermal would be performed as a post-synthesis treatment to achieve particles of well-defined size and morphology. Also, synthesized particles will be dispersed into its colloidal form, and their hydrodynamic sizes would be measured and compared to their microscopy sizes. These nanoparticles will then be further characterized for their crystallinity, purity and other morphological properties.

## 2 Materials and methods

### 2.1 Chemical precipitation synthesis of hydroxyapatite nanoparticles

Chemical precipitation is performed by first preparing aqueous solutions of calcium nitrate tetrahydrate [$Ca(NO_3)_2{\cdot}4H_2O$] (Alfa Aesar, USA) (4.704 g in 50 mL de-ionized water) and ammonium dihydrogen phosphate [$NH_4H_2PO_4$] (Sigma Aldrich, USA) (1.375 g in50 mL de-ionized water). 21.7 mL of 25% v/v ammonium hydroxide [$NH_4OH$] (Merck, Germany) was pre-added to calcium nitrate solution to raise the pH to 11 prior to the precipitation of hydroxyapatite. Ammonium dihydrogen phosphate solution was added drop wise to the alkaline calcium nitrate solution, stirring in a round-bottom flask at room temperature (25 °C). The precipitates formed were then aged in mother liquor for different periods of time (1, 3, 6, 24 and 96 h) before washing five times with de-ionized water to remove all by-products. The synthesized particles were then characterized accordingly.

The above synthesis was repeated at various temperatures (5, 40, 60 and 80 °C) for 24 h to study the effect of synthesis temperature on particle size. Synthesis temperatures, above room temperature, were controlled through the use of a silicone oil bath heated using a heat-controllable magnetic stirrer. For synthesis at 5 °C, a melting-ice bath was used. All samples were stirred throughout the synthesis and the temperatures were monitored using a mercury thermometer to be within ±3 °C.

### 2.2 Hydrothermal of synthesized hydroxyapatite nanoparticles

Hydrothermal was performed on the hydroxyapatite nanoparticles synthesized at various temperatures. For hydrothermal, 15 mL (5 mg/mL) of hydroxyapatite suspension was introduced into the hydrothermal bombs (Parr acid digestion bombs, model 4744), and these bombs were kept in oven at 200 °C for 24 h. After which, the thermally-treated hydroxyapatite suspensions were freeze dried (Alpha 1–4 LSC, Christ, Germany) to obtain the hydroxyapatite powders, which were kept for characterization.

### 2.3 Characterization of hydroxyapatite nanoparticles

Freeze dried hydroxyapatite powders were observed for their particle shape and size on the TEM (2010 TEM, JOEL, Japan) at an accelerating voltage of 200 kV and $LaB_6$ cathode. Samples were prepared by mixing a small quantity of the hydroxyapatite powder in ethanol followed by 10 min of ultrasonic treatment. A carbon coated copper grid was used to collect the samples from the solution and the images were captured via an in-built camera. Particle sizes were measured from TEM micrographs on 200 particles, using the SPOT Basic software.

X-ray diffraction (XRD) was performed using the Shimadzu XRD-6000 Standard employing CuK$\alpha$ radiation ($\lambda$ = 1.5406 Å) at 50 kV and 50 mA. Data were collected over the $2\theta$ range from 10–90° with a step size of 0.05° and scan rate of 5° $min^{-1}$. The infrared spectra of the hydroxyapatite nanoparticles were obtained using the Perkin–Elmer system 2000 FTIR. For FTIR analysis, hydroxyapatite nanoparticles were ground together with oven-dried KBr powder and compressed into a disc. The FTIR spectra were obtained with 16 scans per disc over the range of 4000–400 $cm^{-1}$. The specific surface areas of the synthesized powders were determined by the Brunauer–Emmett–Teller (BET) method using the Micromeritics Surface area analyzer (ASAP 2000, USA).

For hydrodynamic size measurements, colloids of hydroxyapatite nanoparticles were first prepared by dispersing the nanoparticles in solutions of CTAB, SDS or SHMP. CTAB and SDS solutions were prepared at concentrations above their critical micelle concentrations [11], and SHMP solution was prepared at a concentration of 0.1 wt%. After which, 5 mg of HA was added to 10 mL of the dispersant solution and kept in an ultrasonic water bath for 10 min. Hydrodynamic sizes and zeta potentials of the colloids were measured using the ZetaPlus/BI-MAS option (Brookhaven, USA).

## 3 Results and discussion

### 3.1 Chemical precipitation synthesis: effect of synthesis time

The effect of synthesis time on hydroxyapatite nanoparticles was studied at room temperature (25 °C). Figure 1 plots the change in particle size with synthesis time. The results show an increase in particle size with increasing synthesis time, which is similar with the results reported by Saeri et al. [9]. The precipitation of hydroxyapatite nanoparticles can be explained through a crystal nucleation and growth mechanism. During the initial stages of nucleation, a crystal nucleus usually has rough surfaces due to the rapid production of insoluble materials from the supersaturated solution. Over time, this nucleus, with rough surfaces, provides favorable conditions for crystal growth. As a result, crystal growth gives rise to larger particles with increasing synthesis time.

The sizes of these particles were further confirmed by measuring their hydrodynamic sizes. These particles were dispersed in CTAB, SDS and SHMP solutions into colloids before hydrodynamic size measurements were taken. The effectiveness of each of these dispersants was then determined by conducting a simple study of their resultant hydrodynamic sizes, Zeta potentials and colloidal stability under similar conditions, using hydroxyapatite samples synthesized for 24 h. Figure 2 plots the hydrodynamic sizes of the particles in different dispersants over time. The results show that hydroxyapatite nanoparticles dispersed in SHMP had a hydrodynamic size closest to the measured TEM particle size, and also provided the best colloidal stability (Zeta potential = –72 mV) over time. Unlike the organic dispersants (CTAB, SDS) that form micelles, SHMP are adsorbed directly onto the surfaces through an ion exchange mechanism. During ion exchange, the surface phosphate anions are replaced by the anionic phosphate groups of SHMP. The adsorption of the smaller phosphate anions, as compared to the larger micelles, therefore gives rise to a more intimate bonding or adsorption onto the

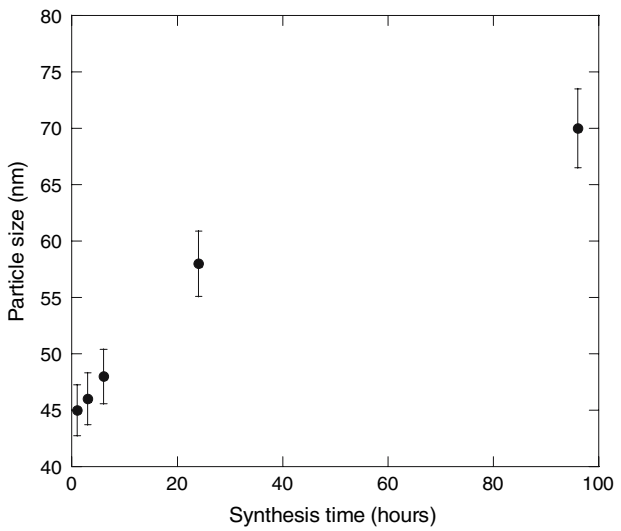


**Fig. 1** Plot of particle size with increasing synthesis time

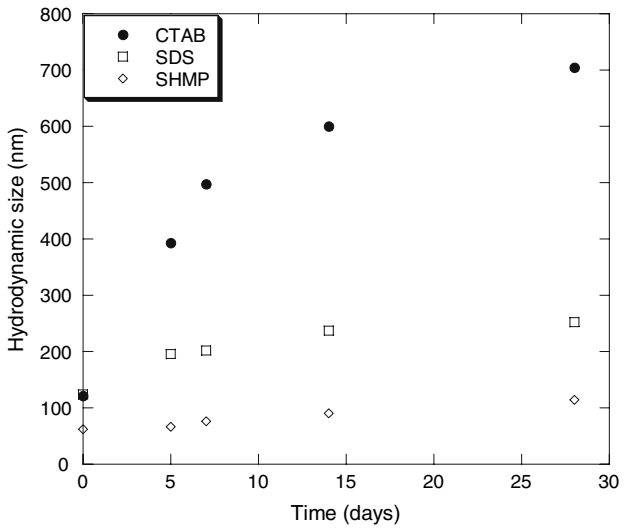


**Fig. 2** Plot of hydrodynamic size of colloidal hydroxyapatite with time

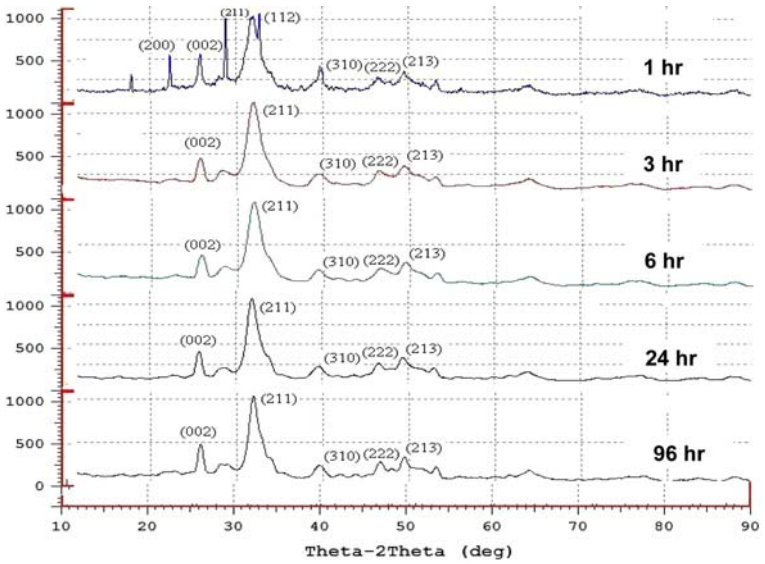


**Fig. 3** XRD patterns of hydroxyapatite synthesized at 25 °C for different synthesis times

particle surface, and possibly resulting in a more stable colloid and a stronger electrostatic repulsion among the particles. As such, SHMP would be used for the dispersion of hydroxyapatite nanoparticles in latter part of the studies, to obtain colloidal hydroxyapatite nanoparticles.

Figure 3 shows the XRD patterns of hydroxyapatite synthesized at different synthesis times. The crystallographic planes corresponding to each XRD peak have been labeled accordingly. The predominant phase was confirmed with JCPDS file no. 09-0432 to be hydroxyapatite. For samples synthesized for 1 h, there were additional peaks present, which corresponded to a small fraction of $\beta$-tricalcium phosphate ($\beta$-TCP) (file no. 09-0169), and these peaks disappeared with longer synthesis time. This suggests that increasing the synthesis time to 3 h and beyond would increase the purity of the hydroxyapatite phase. However, from Fig. 3, contrary to the observation made by Pang and Bao [10], there was no significant evidence that the crystallinity of hydroxyapatite increased with synthesis time. Similar synthesis was also conducted at 80 °C for different times, but there was no distinctive difference in the XRD peaks and crystallinity of the hydroxyapatite nanoparticles, as shown in Fig. 4. This would suggest that firstly, hydroxyapatite synthesized at low temperatures generally results in particles of lower crystallinity; and secondly, increasing synthesis time would have insignificant effects on the crystallinity of particles, regardless of the synthesis temperature.

Figure 5 plots the FTIR spectra of hydroxyapatite synthesized for 1, 24 and 96 h. The spectra contained various peaks from the respective phosphate and hydroxyl groups of hydroxyapatite, which were in

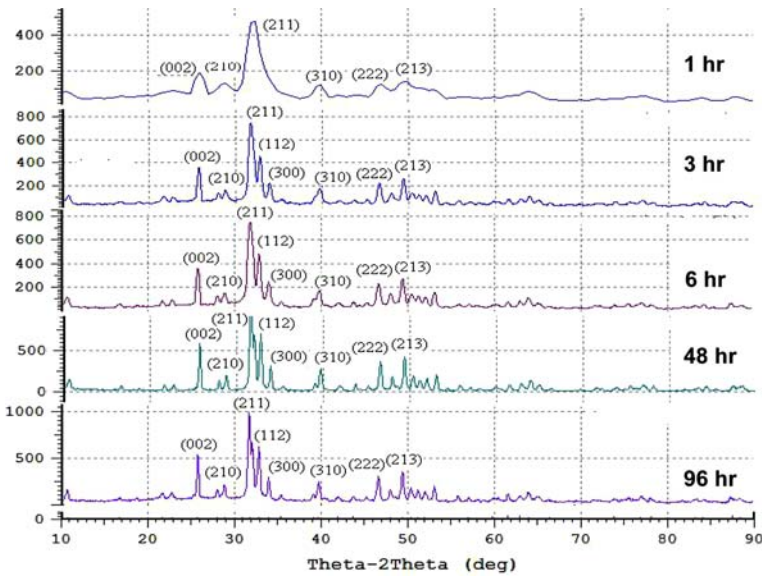


**Fig. 4** XRD patterns of hydroxyapatite synthesized at 80 °C for different synthesis times

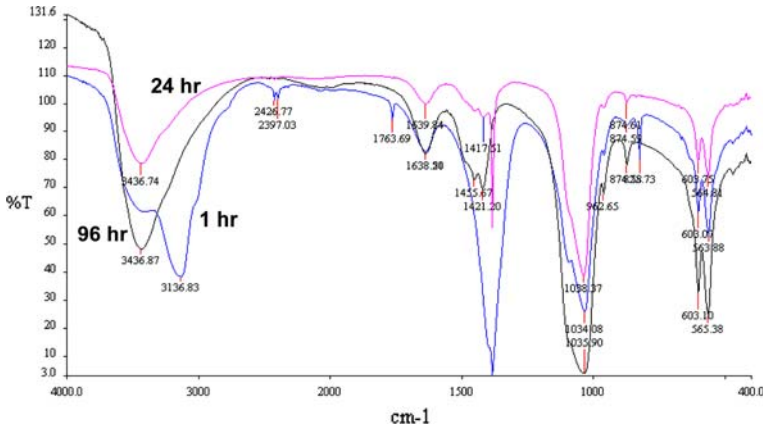


**Fig. 5** FTIR spectra of hydroxyapatite synthesized for 1, 24 and 96 h

agreement to other published data [12]. However, increasing synthesis time resulted in the formation of a peak at 1,423 $cm^{-1}$. The formation of this peak is evidence of a carbonate substitution in hydroxyapatite for particles synthesized for longer time, i.e. 24 and 96 h, though this peak in comparison was less apparent for the 24 h sample. Carbonate substitution in hydroxyapatite probably resulted from the dissolved carbon dioxide from the atmosphere [18], and a longer synthesis time would allow for a greater probability for this substitution to occur. Such a substitution would have important implications of these nanoparticles for targeted-delivery applications, as carbonate-substituted hydroxyapatite would result in a faster dissolution rate in vivo.

### 3.2 Chemical precipitation synthesis: effect of synthesis temperature

The synthesis time of hydroxyapatite was therefore kept at 24 h, since this synthesis time gives particles of a reasonably pure hydroxyapatite phase that is free of other impurities ($\beta$-TCP). The TEM micrographs of the hydroxyapatite nanoparticles obtained at different synthesis temperatures are shown in Fig. 6. The particles were observed to be generally acicular in shape, where particles synthesized at 5 and 25 °C were shorter and thinner (rod-like), whereas particles synthesized at higher temperatures were longer and thicker (plate-like). Particles were also observed to have highly irregular contours, especially for particles synthesized at higher temperatures. From Fig. 6, it

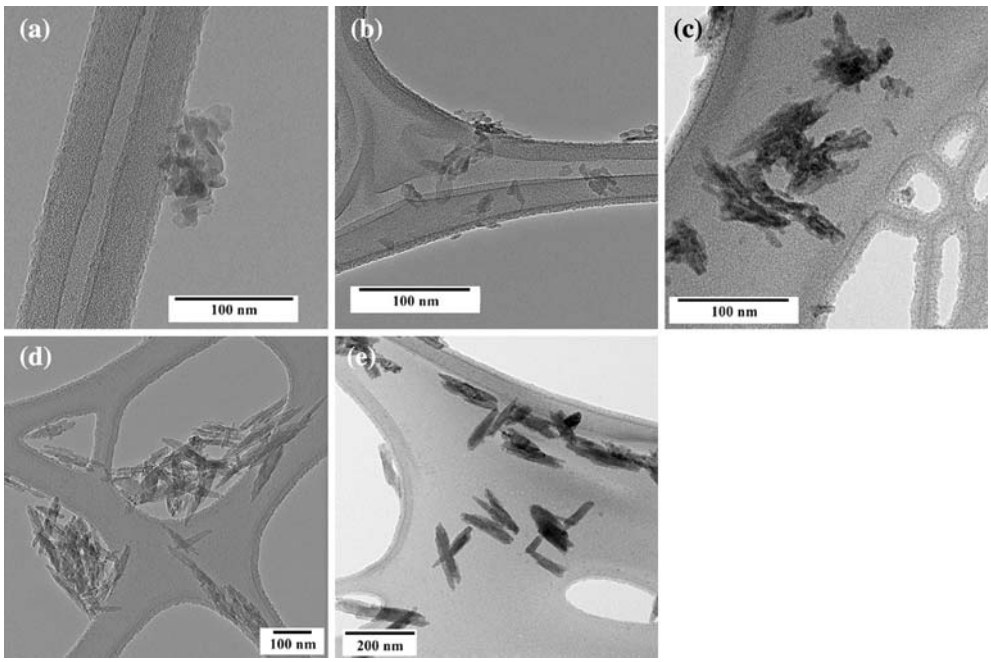


**Fig. 6** TEM micrographs of hydroxyapatite nanoparticles synthesized at (**a**) 5 °C, (**b**) 25 °C, (**c**) 40 °C, (**d**) 60 °C and (**e**) 80 °C

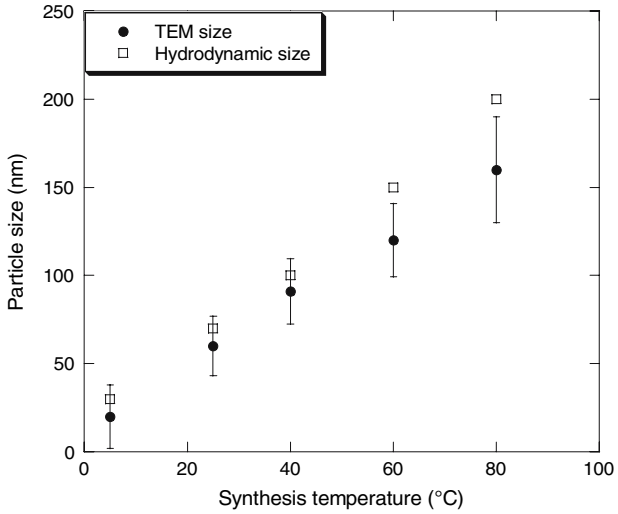


**Fig. 7** Plot of particle size with increasing synthesis temperature

can be observed that particle size increased with increasing temperature, which is in agreement with the observations made by Pang and Bao [10] and Kumar et al. [12]. Close observation of particles synthesized at 5 °C also showed that individual crystallites were around 20 nm in size, which is in agreement with the crystallite size measured by Cao et al. [13] for particles synthesized at this temperature. The acicular particles observed by Cao et al. on the TEM could therefore possibly be due to the directional aggregation of ultra-fine particles (20 nm), as described by Rahaman's classification [17].

The plot of particle size with increasing synthesis temperature is shown in Fig. 7. As before, particle sizes, on the TEM, were measured from the main axis of the nanoparticles with the longer dimension corresponding to the c-axis of the crystal structure. The results show that increasing synthesis temperature resulted in a linear increase in particle size, both for the TEM and hydrodynamic size measurements alike. In general, plate-like morphology will be expected when growth rate is faster, and the observed morphology (Fig. 6) at higher temperatures indicates that growth rate of hydroxyapatite nanoparticles indeed increased with temperature. Therefore, the driving force for the growth of hydroxyapatite increases with temperature [12], which explains for the larger particle sizes at these temperatures. The linear increase in particle size indicates the ability in controlling particle size using temperature as the manipulating parameter. This shows that the size of hydroxyapatite nanoparticles can possibly be tailored and nanoparticles of varying sizes can be obtained. Such control of hydroxyapatite particle size would have tremendous impact for the use of these particles in targeted-delivery applications. However, these particles are observed to have irregular surface contours and as such, its surface morphology is still not quite desirable.

Figure 8 shows the XRD patterns for hydroxyapatite nanoparticles synthesized at different temperatures. It is observed that there was no significant change in the crystallinity of the particles for synthesis temperature lower than 60 °C. However, an increase in crystallinity was observed at 60 °C and above, which was similarly reported by Pang and Bao [10]. The results show that particles synthesized at temperatures below 60 °C results in particles with poor crystallinity, as mentioned earlier, but crystallinity increases and crystallographic orientation improves above this transition temperature. The results

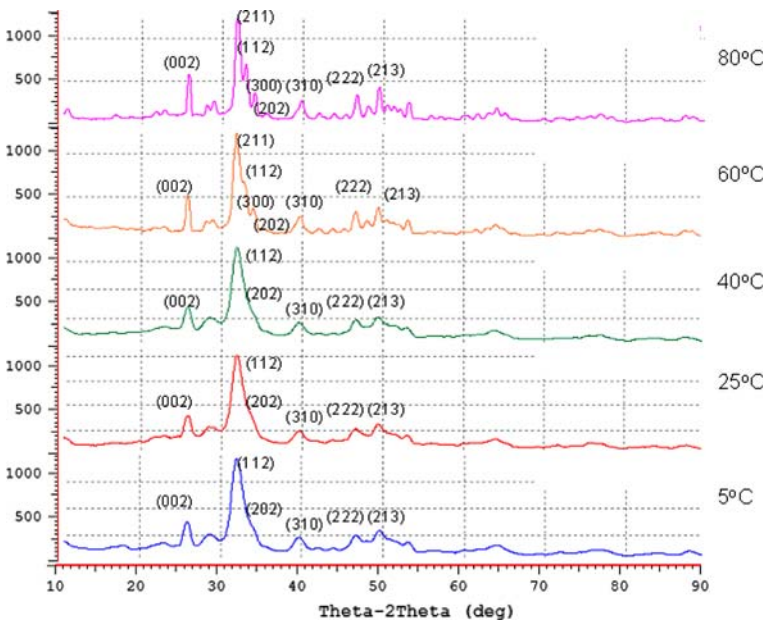


**Fig. 8** XRD patterns of hydroxyapatite synthesized at different temperatures

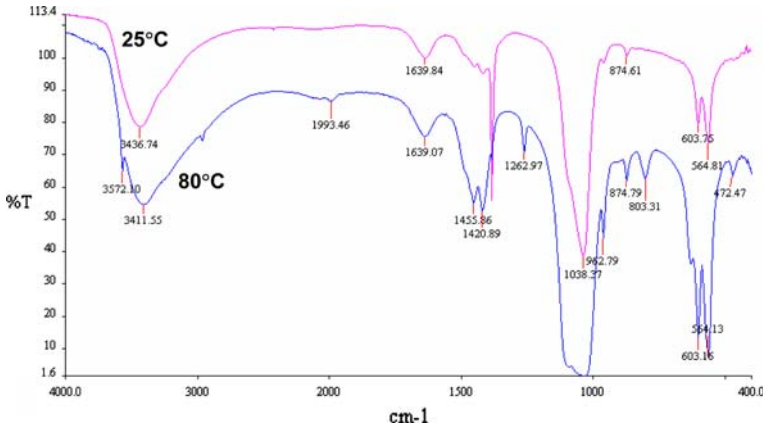


**Fig. 9** FTIR spectra of hydroxyapatite synthesized at 25 and 80 °C

therefore show that synthesis temperature (Fig. 8) has a greater effect on both crystallinity and crystallographic orientation than synthesis time (Fig. 3). This is because temperature is the greater driving force for crystal growth, where higher temperatures would result in particles with larger sizes, higher crystallinity and improved crystallographic orientation.

The FTIR spectra of hydroxyapatite synthesized at 25 and 80 °C is plotted in Fig. 9. The results obtained show that increasing synthesis time increases carbonate substitution of hydroxyapatite as observed from the peaks at 1,423 $cm^{-1}$. This was contrary to the results reported by Kumar et al. [12], who suggested that dissolved carbon dioxide was reduced at higher temperatures. However, we propose that increased carbonate substitution at higher temperatures could be due to the formation of calcium carbonate during the heating of alkaline calcium nitrate solution prior to synthesis, which could have very likely resulted in the formation of carbonate-substituted hydroxyapatite, as observed.

### 3.3 Hydrothermal of hydroxyapatite nanoparticles

Hydrothermal refers to the chemical reaction of substances in a sealed heated solution above ambient temperature and pressure [19], and it allows for the synthesis of fine-grained and highly pure single crystals, with controlled

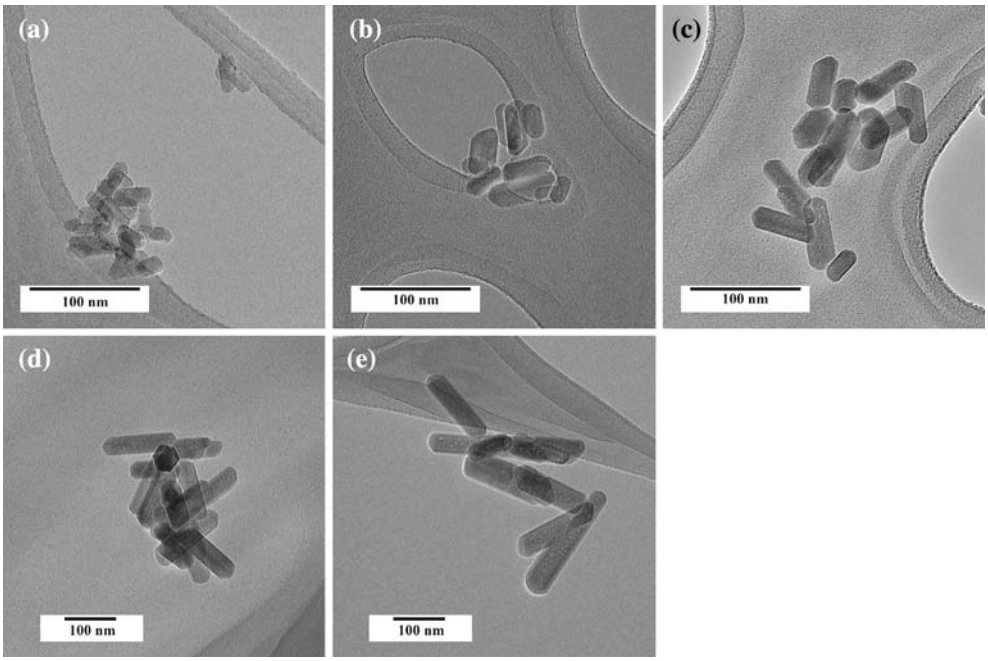


**Fig. 10** TEM micrographs of hydroxyapatite nanoparticles synthesized at (**a**) 0 °C, (**b**) 25 °C, (**c**) 40 °C, (d) 60 °C and (**e**) 80 °C, after hydrothermal

**Table 1** Specific surface area of hydroxyapatite nanoparticles after hydrothermal

| Synthesis temperature | 25 °C | 80 °C |
|---|---|---|
| Without hydrothermal | 79.3 $m^2/g$ | 53.0 $m^2/g$ |
| With hydrothermal | 49.5 $m^2/g$ | 27.5 $m^2/g$ |

morphology and narrow size distribution [20]. Though the size of hydroxyapatite nanoparticles could be controlled by altering the synthesis temperature and time during chemical precipitation, the particles obtained were often irregular in shape and have poor surface morphology (Fig. 6). The employment of hydrothermal would therefore overcome these problems, giving nanoparticles of well-defined sizes and morphology.

Figure 10 shows the TEM micrographs of hydroxyapatite nanoparticles synthesized at different temperatures after hydrothermal. The particles were observed to have more regular shapes and surface contours, and each individual crystal is easily identifiable. The specific surface areas of the hydroxyapatite nanoparticles, before and after hydrothermal, are summarized in Table 1. The results show that the specific surface area decrease after hydrothermal due to the increased regularity of particle morphology, which is consistent with the observation made from the TEM micrographs. The decrease in specific surface area would also imply that hydrothermal-treated particles would have fewer problems with particle agglomeration.

A plot of their particle sizes is shown in Fig. 11. The results, in comparison to Fig. 7, do not show any significant change in the particle sizes after hydrothermal. The plot, on the other hand, does show a strong linear correlation that exists between particle size and synthesis temperature. Hydroxyapatite nanoparticles with well-defined sizes can therefore be tailored using synthesis temperature as the controlling parameter.

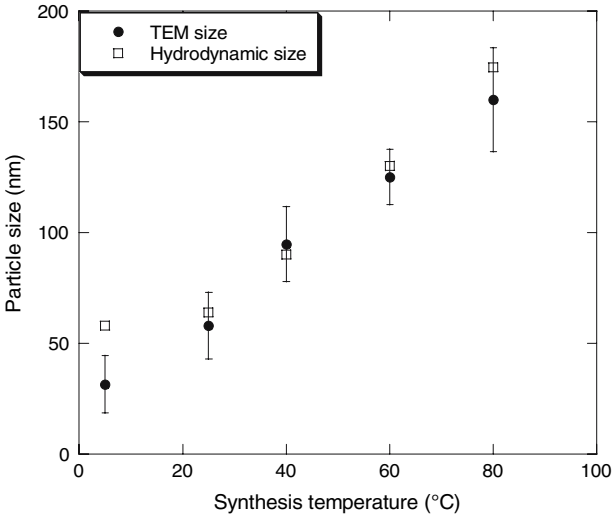


**Fig. 11** Particle size of hydroxyapatite nanoparticles synthesized at different temperatures after hydrothermal

The XRD patterns of hydrothermal treated hydroxyapatite nanoparticles are shown in Fig. 12. Hydrothermal treatment was observed to drastically increase the crystallinity of the particles, as shown from the formation of a peak corresponding to the (300) Miller's plane, for the 25 °C sample. However, there was no distinctive difference for the 80 °C sample. No significant difference was, however, observed for the FTIR spectra of the hydrothermal-treated hydroxyapatite nanoparticles.

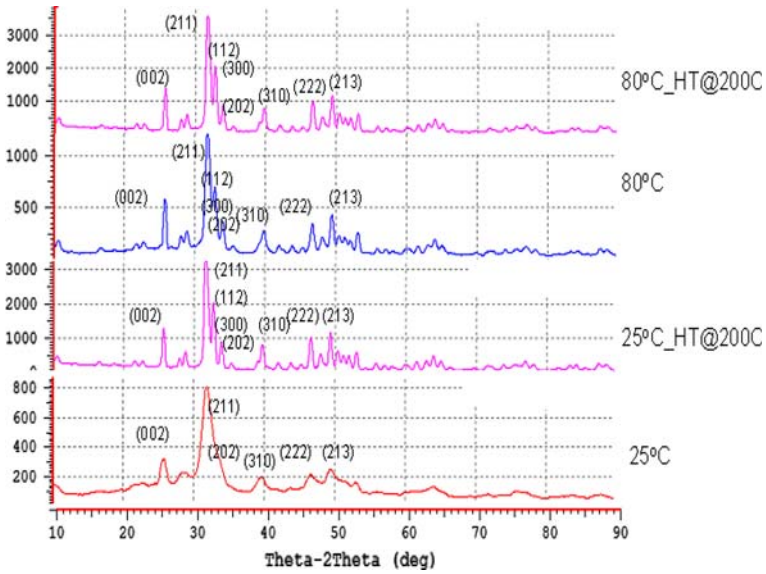


**Fig. 12** XRD patterns of hydroxyapatite nanoparticles after hydrothermal

## 4 Conclusions

The size of hydroxyapatite nanoparticles was shown to increase with increasing synthesis temperature and time. Particle sizes were measured using TEM and DLS measurements, and size was observed to increase linearly with synthesis temperature. Increasing temperature also increases the crystallinity and carbonate-substitution of the synthesized nanoparticles. Hydrothermal of these particles improves particle morphology, giving particles with regular surface contours, well-defined sizes, and possibly, lower particle agglomeration. By controlling synthesis temperature and time, hydroxyapatite nanoparticles with well-defined sizes and morphology can be obtained through chemical precipitation and a post-synthesis hydrothermal treatment.

## References

1. J. CURREY, *Nature* **414** (2001) 699
2. A. KRAJEWSKI, A. RAVAGLIOLI, E. RONCARI, P. PINASCO and L. MONTANARI, *J. Mater. Sci. Mater. Med.* **11** (2000) 763
3. W. PAUL and C. P. SHARMA, *J. Mater. Sci. Mater. Med.* **10** (1999) 383
4. C. C. RIBEIRO, C. C. BARRIAS and M. A. BARBOSA, *Biomaterials* **25** (2004) 4363
5. P. N. KUMTA, C. SFEIR, D. H. LEE, D. OLTON and D. CHOI, *Acta Biomater.* **1** (2005) 65
6. V. S. KOMLEV, S. M. BARINOV and E. V. KOPLIK, *Biomaterials* **23** (2002) 3449
7. G. STORM, S. O. BELLIOT, T. DAEMEN and D. D. LASIC, *Adv. Drug Del. Rev.* **17** (1995) 31
8. I. BRIGGER, C. DUBERNET and P. COUVREUR, *Adv. Drug Del. Rev.* **54** (1995) 631
9. M. R. SAERI, A. AFSHAR, M. GHORBANI, N. EHSANI and C. C. SORRELL, *Mater. Lett.* **57** (1995) 4064
10. X. Y. PANG and X. BAO, *J. Eur. Ceram. Soc.* **23** (2003) 1697
11. T. WELZEL, W. MEYER-ZAIKA and M. EPPLE, Chem. Commun. (2004) 1204
12. R. KUMAR, K. H. PRAKASH, P. CHEANG and K. A. KHOR, *Langmuir* **20** (2004) 5196
13. L. Y. CAO, C. B. ZHANG and J. F. HUANG, *Matl. Lett.* **59** (2005) 1902
14. E. BOUYER, F. GITZHOFER and M. I. BOULOS, *J. Matl. Sci.: Matl. Med.* **11** (2000) 523
15. Y. K. LIU, D. D. HOU and G. H. WANG, *Matl. Chem. Phys.* **86** (2004) 69
16. A. SLOSARCZYK, Z. PASZKIEWICZ and C. PALUSZKIEWICZ, *J. Molec. Struct.* **744–747** (2005) 657
17. M. N. RAHAMAN, *Ceramic Processing and Sintering* (Marcel Dekker: New York, 1995)
18. S. KOUTSOPOULOS, *J. Biomed. Matl. Res.* **62** (2002) 600
19. S. H. FENG and R. R. XU, *Acc. Chem. Res.* **34** (2001) 239
20. K. BYRAPPA, Handbook of Hydrothermal Technology: A Technology for Crystal Growth and Materials Processing (Noyes Publications: New Jersey, 2002)